HHS Public Access

Author manuscript

Cancer Res. Author manuscript; available in PMC 2020 December 15.

Published in final edited form as:

Cancer Res. 2020 June 15; 80(12): 2689–2702. doi:10.1158/0008-5472.CAN-20-0435.

A SIX1/EYA2 small molecule inhibitor disrupts EMT and metastasis

Hengbo Zhou[1,2], **Melanie A. Blevins**[3], **Jessica Y. Hsu**[1], **Deguang Kong**[1], **Matthew D. Galbraith**[1], **Andrew Goodspeed**[1,4], **Rachel Culp-Hill**[3], **Michael UJ. Oliphant**[1], **Dominique Ramirez**[5], **Lingdi Zhang**[3], **Jennyvette T. Pineiro**[3], **Lesley Mathews Griner**[6], **Rebecca King**[6], **Elena Barnaeva**[6], **Xin Hu**[6], **Noel T. Southall**[6], **Marc Ferrer**[6], **Daniel L. Gustafson**[4,5], **Daniel P. Regan**[4,5], **Angelo D'Alessandro**[3], **James C. Costello**[1,4], **Samarjit Patnaik**[6], **Juan Marugan**[6], **Rui Zhao**[3,*], **Heide L. Ford**[1,4,*]

[1]Department of Pharmacology, University of Colorado Anschutz Medical Campus, Aurora, Colorado, USA

[2]Cancer Biology Program, University of Colorado Anschutz Medical Campus, Aurora, Colorado, USA

[3]Department of Biochemistry and Molecular Genetics, University of Colorado Anschutz Medical Campus, Aurora, Colorado, USA

[4]University of Colorado Cancer Center, University of Colorado Anschutz Medical Campus, Aurora, Colorado, USA

[5]Flint Animal Cancer Center, Colorado State University, Fort Collins, Colorado, USA

[6]Early Translation Branch, National Center for Advancing Translational Sciences, National Institutes of Health, Rockville, Maryland, USA

Abstract

Metastasis is the major cause of mortality for cancer patients, and dysregulation of developmental signaling pathways can significantly contribute to the metastatic process. The SIX1/EYA transcriptional complex plays a critical role in the development of multiple organs and is typically downregulated after development is complete. In breast cancer, aberrant expression of SIX1 has been demonstrated to stimulate metastasis through activation of TGF-β signaling and subsequent induction of epithelial-mesenchymal transition (EMT). In addition, SIX1 can induce metastasis via non-cell autonomous means, including activation of GLI-signaling in neighboring tumor cells and activation of VEGF-C-induced lymphangiogenesis. Thus, targeting SIX1 would be expected to inhibit metastasis while conferring limited side effects. However, transcription factors are notoriously difficult to target, and thus novel approaches to inhibit their action must be taken. Here we identified a novel small molecule compound, NCGC00378430 (abbreviated as 8430), that reduces the SIX1/EYA2 interaction. 8430 partially reversed transcriptional and metabolic profiles

Corresponding authors: Heide L. Ford, University of Colorado Anschutz Medical Campus, 12800E. 19th Ave, P18-6115, Mail Stop 8303, Aurora, CO 80045. Phone: 303-724-3509; Heide.Ford@cuanschutz.edu. Rui Zhao, University of Colorado Anschutz Medical Campus, 12801 E. 17th Ave, L18-9111B, Mail Stop 8101, Aurora, CO 80045. Phone: 303-724-3269; Rui.Zhao@cuanschutz.edu.
*Co-corresponding authors.

The authors declare no potential conflicts of interest.

mediated by SIX1 overexpression and reversed SIX1-induced TGF-β signaling and EMT. 8430 was well tolerated when delivered to mice and significantly suppressed breast cancer-associated metastasis in vivo without significantly altering primary tumor growth. Thus, we have demonstrated for the first time that pharmacological inhibition of the SIX1/EYA2 complex and associated phenotypes is sufficient to suppress breast cancer metastasis.

Introduction

High toxicity and low specificity of standard chemotherapy dramatically affects quality of life for cancer patients, necessitating the development of targeted therapeutics. To date, significant advances have been made in the development and use of inhibitors that disrupt kinases that mediate oncogenic signaling, in large part due to the feasibility of targeting ATP-binding pockets in protein kinases. Kinase inhibitors have been shown to improve clinical outcomes in many cancer types. However, resistance frequently develops in patients treated with such inhibitors (1, 2), making it important to develop novel, additional targeted therapies. Recently, oncology has moved towards drugs that activate the immune system as a means to inhibit tumor progression. Unfortunately, such therapies are effective only in a small population of patients, and can cause severe side effects (3). In contrast, few therapies are being developed that target metastasis specifically, which is the main cause of the vast majority of cancer deaths. It is thus critical to continue to explore novel approaches that inhibit tumor progression, with a specific emphasis on the development of drugs that target metastatic disease.

The fundamental molecular principles of cancer, including loss of growth inhibition, sustained proliferative signaling, unlimited replicative potential, and evasion of apoptosis, often result from dysregulated transcription (4). Although specific transcription factors have been identified as essential to the induction of tumorigenesis and metastasis, few drugs target these critical regulators. Instead, most anti-cancer drugs target binding pockets in enzymes or on protein receptors. These drugs often target upstream pathways that can cripple tumors, but may fail to hit the central node (such as a transcription factor) that responds to multiple oncogenic signals. Thus, it is essential to investigate the more difficult task of targeting the transcription factors themselves (either directly or via targeting their regulation), particularly those that are involved in the metastatic process.

The Sine oculis homeobox homolog 1 (SIX1) is a homeoprotein (5, 6) that transcriptionally controls the expansion of progenitor cell populations through its effects on proliferation and survival, and that also controls cell migration, invasion, and epithelial to mesenchymal (EMT) transitions during the embryonic development of numerous organs (5, 7, 8). SIX1 is largely downregulated post-embryogenesis, but is re-expressed in a number of cancers where it is known to contribute to tumor growth and progression (9–13), likely through reinstating embryonic properties out of context. Intriguingly, gain-of-function mutations in Six1 were recently described in Wilms tumors (14, 15), with mutations increasing the ability of SIX1 to transcriptionally activate glycolytic genes, thereby potentiating the Warburg effect (16). While gain-of-function SIX1 mutations have not been observed in breast cancer (13), it is amplified in a small percentage of breast tumors (17), and is overexpressed in up to 90% of

all breast cancers regardless of subtype when compared to normal breast tissue (13, 17, 18). Using xenograft and transgenic mouse models, we and others have shown that SIX1 is a critical mediator of cancer onset and progression (11, 19–23), and that it enhances metastasis via multiple mechanisms, both tumor cell autonomous and non-cell autonomous (24). It is becoming increasingly appreciated that targeting transcription factors (TFs) will be critical in the fight against cancer, and SIX1 has been highlighted as a key candidate to target to inhibit EMT and tumor progression (25).

SIX1 contains a DNA-binding homeodomain, but does not harbor an intrinsic transactivation domain (5). Developmentally, SIX1 partners with eyes absent (EYA) family members, which function as transcriptional coactivators to form a bipartite transcriptional complex (8). Importantly, SIX1 requires its interaction with EYA proteins to mediate metastasis (26, 27). Like SIX1, EYA proteins are largely downregulated post-embryogenesis (28–30) but are re-expressed in cancers (5, 26, 27, 31). Thus, targeting the SIX1-EYA transcriptional complex may be a means to inhibit tumor progression without inducing significant side effects given the low expression of these proteins after development is complete. Herein, we describe our identification and development of a novel small molecule compound, NCGC00378430 (abbreviated as 8430), that reduces the SIX1-EYA2 interaction in cells. Compound 8430 partially reverses the transcriptional and metabolic effects observed by SIX1 overexpression, and also reverses SIX1-induced TGF-β signaling and EMT *in vitro* in breast cancer cells. Most importantly, 8430 had little toxicity *in vivo*, yet dramatically impeded SIX1-induced breast cancer metastasis in a mouse model of breast cancer. Taken together, our work provides proof-of-concept data that SIX1, and thus likely other transcription factors, can be promising pharmacologic targets to suppress tumor progression.

Methods

Biological and Technical Replicates in Experiments

With the exception of RNA-sequencing, metabolomics and animal studies, all experiments were independently conducted in triplicates 3 or more times. Images and quantification from individual representative experiments were shown to reflect the intrinsic variability of each assay. Biological triplicates were used for RNA-sequencing and metabolomics analyses. The animal study using MCF7 tumor xenografts in NSG mice was performed twice using exactly the same conditions (n= number of mice per group per experiment), and results were combined for analysis.

Survival Analysis in TCGA BRCA patients

Median-centered log2 transformed mRNA expression and corresponding clinical BRCA data were obtained from the curated TCGA PanCancer Atlas study dataset via the cBioPortal cgdsr R package (https://cran.r-project.org/web/packages/cgdsr/index.html). Patients were stratified based on histological subtype, and further stratified by combined SIX1 and EYA2 expression status according to percentile cut-offs. Survival analysis was performed using the R packages “survival” and “survminer” (https://cran.r-project.org/web/packages/survival/index.html). Patients exhibiting high SIX1 and EYA2 expression were assigned “BOTH HIGH” status and patients exhibiting any other combination of SIX1 and

EYA2 (both low, only high SIX1, and only high EYA2) were assigned “OTHER” status. To prevent the arbitrary selection of a percentile from which to stratify patients into the aforementioned SIX1/EYA2 covariate groups, we iterated a log-rank test (constructed under a Cox proportional hazards model) and obtained *p*-values with SIX1/EYA2 status as the covariate at all discrete percentiles from the 1–100th percentiles. Representative Kaplan Meier curves reported in this manuscript are based on a range of percentile cut-offs which yielded adjusted p-values≤0.05 when the log-rank test was performed.

Protein expression and purification

Human SIX1 (residues 1–259) was subcloned into the pET21a vector modified to include the DNA sequence for GST and expressed in the BL21(DE3) *E. Coli* strain (Novagen). GST-fused SIX1 was purified from the lysate using Glutathione Sepharose 4B resin, and washed with Buffer L (100 mM Tris-HCl pH 8.0, 250 mM NaCl, 5% glycerol, and 1 mM TCEP) before elution by Buffer L containing 30 mM glutathione and 0.1% Triton X. After concentration, SIX1 was further purified on a Superdex 200 size exclusion column (GE Healthcare).

Human EYA2ED (residues 253–538) was subcloned into the pET15b vector. 6xHis-EYA2 ED was expressed in the BL21(DE3) *E. coli* strain (EMD Biosciences). Cells were lysed by sonication in Buffer L. 6xHis-EYA2 ED was purified using Ni2+-Sepharose HP resin (GE Healthcare). Bound protein was washed with 60 mM imidazole in Buffer L and eluted using an imidazole gradient up to 1 M imidazole. Eluate from the Ni2+ resin was concentrated and further purified on a Superdex 200 size exclusion column (GE Healthcare) in Buffer L.

AlphaScreen Assay

The AlphaScreen assay was carried out using 6xHis-EYA2 ED and GST-SIX1 proteins as previously described (32). Briefly, the assay was carried out in white 384-well plates (PerkinElmer) at 25 °C in assay buffer (50 mM Tris [pH 8.0], 250 mM NaCl, 0.05% bovine serum albumin [BSA], and 0.02% Tween-20). Compounds of varying concentrations (781 nM–100 μM) were incubated for 2 h with 200 nM 6xHis-EYA2 and 200 nM GST-SIX1 before the assay plate was read in an EnVision Multilabel Reader (PerkinElmer) in AlphaScreen detection mode. The IC_{50} value of each compound was calculated using non-linear regression (dose-response inhibition module) in the GraphPad Prism software.

NCGC00378430 synthesis

The synthesis of NCGC00378430 was initiated by the nucleophilic substitution of 2-methoxy-5-nitrobenzenesulfonyl chloride with morpholine followed by a palladium-on-carbon catalyzed hydrogenation of the nitro group to the aniline. This aniline was then subjected to HATU-mediated amide coupling with commercially available 3-(1H-pyrrol-1-yl)benzoic acid to provide NCGC00378430 (N-(4-methoxy-3-(morpholinosulfonyl)phenyl)-3-(1H-pyrrol-1-yl)benzamide). For a more detailed analysis of this synthesis, please see supplementary methods.

Cell culture

Detailed cell culture conditions for all breast cancer cell lines are described in the supplementary methods. HMLER cell line is a kind gift from Robert Weinberg at MIT. MCF7, T47D and MDA-MB-231 cells have been used in the Ford lab since its inception, the same lines can be obtained from ATCC HTB-22, ATCC HTB-133 and ATCC HTB-26, respectively. MCF7-Ctrl and MCF7-SIX1 cells were generated as described before (27). All cell lines were authenticated by University of Colorado Cancer Center Protein Production, Monoclonal Antibody, Tissue Culture Shared Resource using STR analysis (latest authentication was performed on 10/25/2019). All cells are examined by MycoAlert Mycoplasma Detection Kit (Lonza LT07–118) bi-monthly and only negative cells were used for experiments.

Western Blotting

Cells were detached and whole-cell protein extracts were isolated by lysing cell pellets using RIPA buffer. Collected protein lysates (30–50 μg) were run through polyacrylamide gel electrophoresis, size-separated proteins were then transferred to nitrocellulose membranes followed by the blocking step using 5% non-fat milk. Next, membranes were incubated with the primary antibodies for overnight at 4°C. The following day, membranes were washed with TBST and secondary antibodies were applied. Finally, membranes were washed and examined using chemiluminescence which were then imaged on the Odyssey Fc Imaging System (LI-COR Biosciences). Antibodies and concentrations that were used are outlined in Supplementary table 1.

Immunoprecipitation

Cells were lysed using ELB buffer (250mM NaCl, 50mM Hepes pH 7.0, 5mM EDTA and 0.1% NP40), and protein samples were pre-cleared using TrueBlot anti-Rabbit IgG Magnetic beads (Rockland p/n 00–1800-50). Samples were then incubated with 2μg of antibody targeting EYA2: anti-EYA2 IgG (Sigma, HPA027024) and 50μl of Trueblot magnetic beads overnight at 4 °C, while gently rocking. The following day, beads were washed using TBS, and proteins were dissociated from the beads by boiling the sample with loading buffer prior to the Western Blotting analyses. Of note, secondary antibodies used during Western Blot analyses only recognize non-denatured IgG (Rabbit Trueblot Anti-Rabbit IgG HRP, Rockland, p/n 18–8818-31) and Mouse Trueblot ULTRA Anti-Mouse IgG HRP, Rockland, p/n 18–8817-33).

Proximity Ligation Assay (PLA)

Cells were incubated in 4% paraformaldehyde for 15 minutes, and were then permeabilized using 2% Triton in PBS. The Duolink In Situ Red Starter Kit Mouse/Rabbit (Sigma Aldrich, DUO92101) was used to perform PLA following the manufacturer's instructions. The SIX1-EYA2 interaction was detected using the antibody pairs listed below, and examined by fluorescent microscopy. Antibody pairs: anti-SIX1 IgG (Cell Signaling, D4A8K, 1:50) and anti-EYA2 IgG (Sigma Aldrich, WH0002139M4, 1:50). Finally, PLA signal was quantified using Cellprofiler software and calculated as the ratio of red fluorescence over DAPI signal. One-way ANOVA with Tukey post-test was applied for statistics analysis. For

quantification, more than 200 cells from 5 fields per condition were examined in each experiment.

MEF3 Firefly/Renilla Dual luciferase assay

Cells were transfected with the PGL3 Renilla reporter vector (as a control for transfection efficiency) along with either PGL3 empty vector (EV) or PGL3 MEF3 Firefly reporter (33) for 48 hours in triplicate. After 48h, vehicle (DMSO) or 8430 treatment at the mentioned doses was administered for 1 day prior to luciferase activity measurement. Renilla and Firefly luciferase activity was measured following protocols provided in the Dual-Luciferase Reporter Assay System (Promega, E1960), and data was collected using a Modulus II Microplate Multimode Reader (Promega, 998–9375). All Firefly/Renilla ratios were normalized to the empty vector with vehicle treatment condition.

Immunocytochemistry

Cells were fixed in 4% paraformaldehyde for 15 minutes and permeabilized using 2% Triton in PBS for 10 minutes, after which they were blocked with 10% goat serum for 30 minutes. Primary antibodies were applied for an overnight incubation at 4 °C. The following day, primary antibody was removed and three times of PBS wash was performed. Then, secondary antibodies were applied for 1 hour followed by PBS wash and slides were mounted using Fluoroshield with DAPI (Sigma Aldrich, F6057–20ML) prior to quantitation using fluorescent microscopy. Quantification was performed using the Cellprofiler software, where the percentage of high junctional E-cadherin was assessed using number of cells with strong membranous E-cadherin expression (fluorescent intensity at 30% greater than cytosolic signal) over total cell number, while Fibronectin expression was assessed by ratio of total red fluorescence intensity over DAPI. Similar to PLA, more than 200 cells from 5 fields per condition were examined in each experiment. Antibodies and concentrations that were used are outlined in Supplementary table 1.

RNA sequencing

Total RNA was isolated from MCF7 cells using Direct-zol RNA Miniprep Kit (Zymo Research R2052), RNA integrity and purity was checked by agarose gel electrophoresis and NanoDrop 2000 spectrophotometer (ThermoFisher ND-2000) prior to sample submission. RNA samples with high integrity (>95%) in biological triplicates were submitted to submitted to Novogene (Beijing, China) for library preparation and high-throughput sequencing, using the NEBNext Ultra RNA library Prep kit and Illumina NovaSeq 6000 S4 platform.

RNA-seq data analysis

NovaSeq Control Software (Illumina) was used for signal processing, base-calling and removal of barcode and adapter sequences. Data quality was assessed using FASTQC (version 0.11.5, https://www.bioinformatics.babraham.ac.uk/projects/fastqc/) and FastQ Screen (v0.9.1) was used to check for common sequencing contaminants (https://www.bioinformatics.babraham.ac.uk/projects/fastq_screen/). Low quality bases (Q <10) were trimmed from the 3’ end of reads and reads (<30 nt after trimming) were removed

using the Fastx toolkit. Reads were aligned to a GRCh37/hg19 Human reference using TopHat2 (v2.1.1, --b2-sensitive --keep-fasta-order --no-coverage-search --max-multihits 10 --library-type fr-firststrand) with the UCSC hg19 GTF annotation file provided in the iGenomes UCSC hg19 bundle (https://support.illumina.com/sequencing/sequencing_software/igenome.html). Aligned reads were then filtered to remove low quality mapped reads (MAPQ < 10) using SAMtools (v1.5). Quality assessment of final mapped reads was conducted using RSeQC (v2.6.4). Gene-level counts were obtained using HTSeq (v0.8.0) with the following options (--stranded=reverse –minaqual=10 –type=exon –idattr=gene_id --mode=intersection-nonempty) using the iGenomes UCSC hg19 GTF annotation file. Differential gene expression was evaluated using DESeq2 (version 1.6.3) (34) in R (version 3.1.0) using p-adj<0.1 as the cutoff.

Heatmap, ORA, GESA, and GO analysis

To generate heatmaps, significantly differentially expressed genes from between the WT and SIX1 overexpression (OE) condition, as defined by p-adj < 0.1 and $|\log_2$fold-change$| > 1$, were plotted as heatmaps across all RNAseq samples. Gene expression was converted into z-scores prior to plotting, and heatmaps were subsequently created using the package pheatmaps in R (https://cran.r-project.org/web/packages/pheatmap/pheatmap.pdf). Hierarchical clustering of z-score-converted expression values indicates three predominant and distinct clusters of differential gene expression exist. Pathway analysis was performed using gene sets from the Hallmarks collection of the Molecular Signatures Database (35). Over-representation analysis was performed on all genes with a p-adj <0.1 using the clusterProfiler R package (36). Gene set enrichment analysis was performed on the fold-change of the indicated comparisons using the fgsea R package (https://doi.org/10.1101/060012). Gene ontology enrichment analysis was performed on genes influenced by both SIX1 OE and 8430 treatment (p-adj <0.1, and changed in opposite directions) using PANTHER Overrepresentation Test against Homo sapiens GO biological process complete annotation data set (http://geneontology.org/, test type: Fisher's Exact, correction: calculate false discovery rate).

Metabolomics

Metabolomics analyses were performed via ultra-high pressure-liquid chromatography-mass spectrometry (UHPLC-MS – Vanquish and Q Exactive, Thermo Fisher) as previously reported (Nemkov et al., 2015). Briefly, cells (in biological triplicates) were extracted in ice cold methanol:acetonitrile:water (5:3:2 v/v) at a concentration of 2 million cells/ml. After vortexing for 30 min at 4°C, samples were centrifuged at 15,000 g for 10 min at 4°C and supernatants processed for metabolomics analyses. Ten microliters of sample extracts were loaded onto a Kinetex XB-C18 column (150 × 2.1 mm i.d., 1.7 μm – Phenomenex). A 5 min gradient was used to elute metabolites for both negative mode (phase A: 5% acetonitrile 95% water with 1mM ammonium acetate and B: 95% acetonitrile 5% water with 1mM ammonium acetate, 0–100%B) and positive mode (phase A: 0.1% formic acid in water, phase B: 0.1% formic acid in acetonitrile, 5–95% B). The mass spectrometer scanned in Full MS mode at 70,000 resolution in the 65–975 m/z range, 4 kV spray voltage, 45 sheath gas and 15 auxiliary gas, operated in negative and then positive ion mode (separate runs). Metabolite assignment was performed against an in-house standard library, as reported (37).

Immunohistochemistry

Immunohistochemical staining was performed by the University of Colorado Cancer Center Histology Shared Resource using a previously described procedure (33). Sections were examined through bright-field microscopy and signal positive regions (staining intensity 50% greater than background) were quantified using ImageJ software. More than 1000 cells from 4 fields per tumor were examined. Antibodies and concentrations that were used are outlined in Supplementary table 1.

Evaluation of 8430 pharmacokinetics

For a detailed analysis of pharmacokinetic evaluation, please see supplementary methods.

Evaluation of 8430 toxicity

8430 was formulated in a mixed solution containing N-Methyl-2-pyrolidone (NMP, Sigma Aldrich, 328634), PEG400 (Sigma Aldrich, 202398) and 30% Solutol® HS 15 w/w in water (Sigma Aldrich, 42966), in a 1:2:3 ratio. NMP, PEG400 and Solutol® HS 15 mixed solvent was used as vehicle control. 8430 was introduced to 4th mammary fat pad of CD-1 mice at 0 (vehicle), 15, 20 and 25 mg/kg every other day for three continuous weeks. Animal weight was measured every week. In addition, animals were euthanized, both gross and histopathological evaluation was performed, including histological assessment of liver, heart, pancreas, small and large intestine tissues by a board-certified veterinary pathologist (DR) at the Comparative Pathology Laboratory at Flint Animal Cancer Center, Colorado State University.

Animal experiment

6–8 week old NSG mice were used for MCF7 tumor cells implantation, respectively. Estrogen pellets were embedded subcutaneously in 6–8 week old NSG mice one day before breast tumor cell injection as previously described (18). The following day, 3×10^5 turboRFP labeled MCF7 SIX1 cells were orthotopically introduced into the 4th mammary fat pad of NSG mice. Vehicle or 25mg/kg of 8430 treatment (adjacent to the injection site of the tumor cells) started 2 days after the injection (day 3), and was continued every other day until the day 21. Fluorescent signal was examined and quantified every week using IVIS 200 (PerkinElmer)-imaging until the end of study (week 9), signal mean was plotted across time, and statistical significance was evaluated using a functional longitudinal mixed-effects model. At the end of study, mice were euthanized while primary tumors were harvested for further immunohistochemical analysis. In addition, multiple organs of the mice were examined during necropsy. However, in this analysis we only observed lymph node metastases (metastases were confirmed by examination of H&E sections by a pathologist, Dr. Paul Jedlicka). All work involving animals was approved by IACUC at University of Colorado, Anschutz Medical Campus.

Results

SIX1/EYA2 complex is a potential therapeutic target for breast cancer

Previous analysis of the van de Vijver gene expression dataset (295 patients) demonstrated that co-expression of SIX1 and EYA2 is significantly associated with poor prognosis in human breast cancer (27). Using the current larger TCGA PanCancer Atlas breast cancer (BRCA) dataset, which contains expression data from 943 breast cancer patients with identified disease subtypes, we asked whether simultaneous high expression of SIX1 and EYA2 are particularly relevant to specific subtypes of the disease. To that end, we used a Cox regression model, stratifying patients based on combined high SIX1 and EYA2 expression (strata definitions described in Methods section) as covariates. Intriguingly, we discovered high expression of SIX1 and EYA2 shows strong predicting power only in luminal A and basal subtypes, but not in other breast cancer subtypes. Particularly, at the most significant cut-off percentile (lowest p value), simultaneous high expression of SIX1 and EYA2 strongly associates with shorter progression free survival in luminal A (55^{th} percentile) and basal (74^{th} percentile) breast cancer patients (Fig. 1). Taken together, these data suggest that the SIX1/EYA2 complex may be an attractive therapeutic target for more than one breast cancer subtype.

Identification of a small molecule compound targeting the SIX1-EYA2 complex

To monitor the ability of SIX1 to interact with its protein partner, EYA2, we developed an AlphaScreen assay amenable to miniaturization for a high throughput screen (HTS) (38). Human EYA2 (residues 253–538) was expressed and purified with a His_6 tag for binding on Ni^{2+}-chelated acceptor beads, while SIX1 (residues 1–259) was expressed and purified as a GST-fusion protein for immobilization on GSH-linked donor beads. The interaction of SIX1 and EYA2 brings the donor and acceptor beads close together and produces strong fluorescent signal. Untagged EYA2, but not an unrelated protein, Brr2, inhibits this signal, indicating that the fluorescent signal is specific to SIX1-EYA2 interaction (Fig. 2a). Screening of ~370,000 compounds from the NIH's Molecular Library Initiative using this AlphaScreen assay identified a class of compounds that inhibited SIX1-mediated transcription by 50% at 50μM concentration in a MEF3-luciferase reporter assay (39) in MCF7 cells (Supp. Fig. 1). Our medicinal chemistry effort around the parental compound generated one analog (NCGC00378430, abbreviated as 8430, Fig. 2b & Supp. Fig. 2a & b) that has a moderate IC50 of 52μM in the Alphascreen assay (Fig. 2c), but improved inhibitory activity against SIX1-mediated transcription (80% inhibition at a concentration of 50μM in the luciferase assay, Fig. 2d). Intrigued by this apparent cellular activity, we decided to further characterize compound 8430 in cell-based assays.

Compound 8430 disrupts the SIX1-EYA2 interaction and transcriptional activity in tumor cells

Because 8430 was able to reduce SIX1-mediated transcription, we set out to evaluate the effects of this compound in a well-characterized breast cancer cell line model, MCF7, where we had previously shown that SIX1 can induce metastasis in a manner dependent on EYA2, via stimulating TGF-β signaling and EMT (26). In addition, in this same MCF7 model, we had demonstrated genetically that disruption of the SIX1-EYA2 interaction, via expression

of an EYA-binding deficient mutant of SIX1 ($SIX1^{V17E}$), led to a significant reduction in SIX1-induced breast cancer metastasis (27). Together, these data provide clear evidence that in the context of MCF7 cells, SIX1 requires EYA2 to mediate metastasis, and thus provides a perfect model in which to test the effect of our inhibitor on metastasis.

To this end, previously generated stable SIX1 overexpressing (OE) MCF7 cells (MCF7-SIX1) were used, while chloramphenicol transferase-OE MCF7 cells (MCF7-Ctrl) were used as control (27). As additional models to examine the efficacy of 8430, we chose two breast cancer cell lines (one hormone positive, T47D, and one triple negative, MDA-MB-231) that expressed high endogenous levels of SIX1 and EYA2 compared to MCF7 and HMLER cells (Supp. Fig. 3). All models were treated with either vehicle (DMSO) or 8430 (10μM for MCF7, and 20μM for T47D as well as MDA-MB-231 cells), and the SIX1-EYA2 interaction was evaluated using a Proximity Ligation Assay (PLA). Strikingly, 8430 effectively decreased the SIX1-EYA2 interaction as measured in PLA, when compared to the vehicle control, in all three systems (Fig. 3a-c).

Because PLA is an indication of proximity, and cannot be used to definitively measure protein-protein interactions (40, 41), we also performed immunoprecipitation (IP) assays to validate the effect of 8430 on the SIX1/EYA2 complex. In corroboration of the PLA results, 8430 dramatically decreased EYA2-associated SIX1 across all three systems (Fig. 3d-f). It should be noted that, in addition to disrupting the interaction, it is possible that 8430 indirectly influences the complex by also affecting protein levels. Importantly, we found that SIX1/EYA2 transcriptional activity is suppressed by 8430 across all three systems (Fig. 3g-i). Thus, our data demonstrate that 8430 can inhibit the SIX1-EYA2 complex, and its transcriptional activity, in breast cancer cells.

Compound 8430 partially reverses SIX1-mediated transcriptional and metabolic signatures in breast tumor cells

Since 8430 reduces the SIX1-EYA2 interaction in cells, we next examined whether this inhibitor could reverse global gene expression changes induced by SIX1 overexpression. To this end, we treated MCF7-Ctrl cells with vehicle (DMSO, abbreviated as Veh), and MCF7-SIX1 cells with vehicle or 10μM 8430 for 3 days, after which we performed RNA isolation and RNA sequencing (RNA-seq) analysis. Comparison of transcriptional profiles between Ctrl+Veh, SIX1+Veh and SIX1+8430 showed that 8191 genes (4048 up and 4143 down) were significantly altered (adjusted p value<0.1) by SIX1 OE (Supp. Fig. 4a **left**), whereas 8430 treatment, compared to Veh treatment, significantly changed 1082 genes (351 up and 731 down) (Supp. Fig. 4a **middle**). Of note, when comparing SIX1+8430 to Ctrl+Veh, there are 7836 genes (3884 up and 3952 down) significantly changed (Supp. Fig. 4a **right**). Although SIX1 long-term OE influences the transcriptional profile of breast cancer cells more profoundly than 8430 treatment, there was a substantial overlap between genes altered by SIX1 OE and 8430 treatment (Fig. 4a, Supp. Fig. 4b). Specifically, 534 of the 1082 genes that were dramatically altered after 8430 treatment were also impacted by SIX1 OE in the opposite direction (up in SIX1 OE and down in 8430 treatment, or vice versa) (Fig. 4a). While 8430 was unable to reverse the full spectrum of gene changes induced by SIX1, it is likely that long term expression of SIX1 in a stable cell line imparts more stable changes

(such as epigenetic alterations) that are not easily reversed by short term treatment of the compound.

Despite 8430 affecting a smaller number of genes than SIX1 OE, we observed marked similarities in the processes/pathways induced by SIX1 and reversed by 8430 treatment. For example, biological processes relevant to development such as cell differentiation, cellular developmental process and tissue development were particularly enriched both with SIX1 overexpression and 8430 treatment (Supp. Fig. 4c), strongly indicating 8430 specifically influences developmental processes which are known to be regulated by the SIX1/EYA2 complex. Through over-representation analysis (ORA), we found substantial overlap (11 out of top 15 enriched pathways) between pathways impacted by SIX1 OE and 8430 treatment (Fig. 4b). In particular, EMT, known to be regulated by SIX1/EYA2 complex (11, 26, 27, 42), ranked high in the overlapping pathways list. In agreement with ORA pathway analysis, Gene Set Enrichment Analysis (GSEA) also demonstrated that SIX1 OE and 8430 treatment influenced EMT in opposite directions (Fig. 4c). Together, through interrogating global transcriptional signatures, we demonstrate that compound 8430 is able to partially reverse SIX1-mediated transcriptional changes, including SIX1-induced EMT gene expression signatures.

Recent studies demonstrated a novel role for SIX1 in enhancing aerobic glycolysis, and thus the Warburg effect, in cancer cells, as a means to promote tumor progression (16, 43, 44). We thus asked whether 8430 treatment would alter the metabolic profile of breast cancer cells by performing metabolomics analysis on MCF7-Ctrl cells treated with vehicle, and MCF7-SIX1 cells treated with vehicle or 8430 at 10μM for 3 days. This analysis revealed that 8430 treatment could partially reverse the metabolic signature induced by SIX1 (Fig. 5a, only top 50 most significantly altered metabolites are shown in heatmap). In particular, TCA cycle intermediates such as malate and fumarate as well as essential amino acids including glutamine, threonine and aspartate were reversed by 8430 (Fig. 5a, black-bracketed regions). Interestingly, 8430 treatment seemed to trigger a strong signature of increased acyl-carnitines which was not observed in other conditions (Fig. 5a, yellow-bracketed region), this could be attributed to 8430-impeded TCA cycle, alternatively, unappreciated effects from 8430 could result in mitochondrial dysfunction that hinders catabolism of fatty acids. In addition, via Metabolites Set Enrichment Analysis (MESA), we discovered a substantial overlap (13 out of 20 top enriched pathways) between pathways altered by SIX1 OE and 8430 treatment (Fig. 5b). Pathways regulated by both SIX1 and 8430 include multiple amino acid synthesis pathways as well as glycolytic pathway. Collectively, 8430 treatment impinges on metabolic pathways regulated by SIX1 OE, and partially reverses the metabolite profile back to that seen in the control condition.

8430 suppresses TGF-β signaling and EMT in breast cancer cells

It is well accepted that SIX1 induces EMT and metastasis, at least in part via its ability to enhance TGF-β signaling (11, 42), and that this effect of SIX1 is mediated by its interaction with EYA2 (26, 27). Further, as mentioned above, our RNA-seq analysis demonstrated that EMT, a major contributor to metastasis (45), is one of top pathways induced by SIX1 and reversed by 8430 treatment. Thus, we asked whether 8430 is able to phenotypically reverse

SIX1/EYA2-mediated induction of TGF-β signaling and EMT in breast cancer cells. To this end, we examined the effects of 8430 in MCF7-SIX1 OE cells, where SIX1 overexpression had previously been shown to increase TGF-β signaling and EMT (11, 26, 27, 42). We also tested 8430 in T47D cells treated with TGF-β to induce an EMT (46, 47).

Strikingly, treatment of MCF7-SIX1 cells with 10μM 8430 reversed the SIX1-induced increase in p-SMAD3 (Fig. 6a), and also led to an alteration in FN1, a well-known mesenchymal marker (Fig. 6b & c). Interestingly, we found that although 8430 treatment did not alter total E-CAD levels (Fig. 6b), it restored membranous E-CAD in MCF7-SIX1 cells, along with inhibiting FN1 expression (Fig. 6c). This phenotype fits well with our previous observation that SIX1 overexpression does not change total E-cadherin levels, but rather changes its localization (11). In T47D cells, 20μM 8430 treatment blocked TGF-β induced activation of p-Smad3, upregulation of FN1, and downregulation of E-CAD (Fig. 6d-e). Similar to what was observed in MCF7 cells, 8430 treatment increased membranous E-CAD expression while decreasing FN1 levels in T47D cells (Fig. 6f). Taken together, 8430 dramatically inhibits TGF-β signaling and EMT in SIX1-high tumor cells.

8430 inhibits metastasis of SIX1 overexpressing tumor cells

Because 8430 reversed the EMT phenotypes induced by SIX1 in breast cancer cells in culture, we examined its effects on SIX1/EYA2 induced metastasis *in vivo*. To this end, we first determined the half-life of 8430 *in vivo*, and found that it was rapidly metabolized, with a half-life under an hour (Supp. Fig. 5a & b). Therefore, we sought out to test whether frequent local delivery would be practical. We examined the maximal dose that could be tolerated in mice, and found no severe toxicity at a dose of 25mg/kg (delivered to 4th mammary fat pad every other day until day 21, performed to mimic our experimental protocol in tumor bearing mice) (Supp. Fig. 5c). Histological examination of organs from non-tumor bearing animals treated with various doses of 8430 did not reveal any major toxicities. The most prominent and frequently observed histological change was the presence of multifocal, random, single cell hepatocyte necrosis in some, but not all, evaluated animals. These foci of necrosis were often associated with a minimal inflammatory response, and rarely, mild replacement fibrosis (Supp. Fig. 5d). The random nature of these lesions suggest they may be embolic in nature, and were interpreted to either reflect an underlying husbandry-related issue or a treatment-related liver toxicity. In those animals bearing histological liver lesions, these lesions were minimal in severity and would be expected to be sub-clinical.

Because we determined that 8430 was relatively safe, we injected 3 × 10^5 turbo RFP-tagged MCF7-SIX1 cells into the 4th mammary fat pad of NOD scid gamma (NSG mice). Two days after tumor cell injection, we treated the mice with vehicle: N-methyl-2-pyrrolidone (NMP), polyethylene glycol (PEG400) and 30% Kolliphor HS15 (Solutol) in 1:2:3 ratio, or 8430 dissolved in the same vehicle. Given the short half-life, the vehicle and compound were delivered to the area adjacent to the site of tumor cell injection every other day until day 21. Although we observed no growth inhibitory effect of 8430 on the primary tumor, 8430 treatment dramatically decreased distant metastatic burden compared to vehicle treatment (Fig. 7a & Supp. Fig. 6a & b), demonstrating the efficacy of this compound as an

anti-metastatic agent. Consistently, immunohistochemistry (IHC) staining of primary tumor sections revealed no proliferative or apoptotic phenotypes when comparing vehicle to 8430 treated tumors (Fig. 7b). Surprisingly, we did observe a slight, yet significant, difference in E-CAD and FN1 expression in the 8430 treated tumors versus their control counterparts (Fig. 7c), even though treatment was stopped at week 3 and the analysis in the tumors was performed 6 weeks after the final injection. These data suggest a prolonged suppressive effect on EMT after short-term treatment of 8430. Thus, although 8430 does not impede primary tumor growth, it greatly hinders metastases development, potentially through long-lasting EMT inhibitory effects. In summary, we have identified a novel compound 8430 that disrupts the SIX1/EYA2 function in cells. Compound 8430 globally acts on numerous transcriptional and metabolic pathways on which SIX1 impinges. Further, consistent with our RNA-sequencing data, we show that 8430 blocks TGF-β signaling and EMT in high SIX1-expressing cells, and most importantly, is able to reverse SIX1-induced metastasis *in vivo* with limited to no toxicity. Thus, our study provides proof-of-concept that pharmacological inhibition of SIX1 is a promising approach to inhibit breast cancer metastasis.

Discussion

Recent advances in targeted therapy have led to improved survival of cancer patients, and have significantly benefitted the breast cancer patient population. However, resistance often develops and cancer re-emerges. Unfortunately, there have been few successful efforts targeting metastasis, and thus many patients succumb to metastatic disease. SIX1, a homeobox transcription factor, requires an interaction with EYA family proteins to transactivate downstream target genes. Concerted high SIX1 and EYA2 expression predicts poor clinical outcome in breast cancer patients harboring tumors of different subtypes (Fig. 1). Importantly, SIX1 promotes tumor progression and metastasis through multiple means, such as inducing TGF-β signaling (11, 42, 48), enhancing VEGF-C production (23, 48), increasing MMP secretion (49, 50), promoting glycolysis (16) and activating GLI signaling in neighboring cells (24). In addition, EYA proteins are known to enhance tumor progression through regulation of migration and invasion of tumor cells (51) as well as through regulating the tumor microenvironment. Because of the many ways by which SIX1 and/or EYA enhance tumor progression, investigating the potential to pharmacologically inhibit their function is of significant value. Since SIX1 and EYA are both developmental genes that are down-regulated in most normal adult tissues (5), inhibiting the SIX1-EYA complex may have limited side effects.

Herein, we identified a promising compound, 8430, that can disrupt SIX1-EYA2 function in cells, and can reverse SIX1-mediated cellular phenotypes and partially restore transcriptional and metabolic signatures that are induced by high SIX1 expression. Most importantly, 8430 inhibits SIX1-mediated breast cancer metastasis in a mouse model. The cellular and *in vivo* effect of 8430 is SIX1-specific, suggesting that the action of the compound is likely to be at least in part through SIX1. However, due to the low potency and solubility of 8430, we have not been able to conclusively demonstrate whether 8430 directly binds to SIX1 and/or EYA2 through *in vitro* biophysical approaches, which typically require high concentrations of interacting partners. Although we demonstrated 8430 disrupts the

SIX1-EYA2 interaction in cells via both PLA and IP analysis (Fig. 3), it remains possible that 8430 reduces the SIX1/EYA2 interaction indirectly in cell culture, for example by affecting the levels of one or both of the proteins. In the future, it will be important to unambiguously identify 8430's direct protein target, either through *in vitro* biochemical analyses as we obtain more soluble and potent compounds, or via the use of affinity tagged analogs for pull down experiments in cells.

RNA-seq analysis revealed that, other than known SIX1-regulated processes such as myogenesis, EMT, TGF-β signaling and Hedgehog signaling, additional pathways are under the control of SIX1 and are targetable through pharmacological inhibition of SIX1 (5). These pathways include estrogen responses, KRAS signaling, apical junction alterations, and hypoxia-associated pathways (Fig. 4b). Further, our metabolomics analysis identified additional metabolic pathways that are under the control of SIX1, beyond its previously reported effects on glycolysis and its association with the Warburg effect (16). For example, multiple amino acid and nucleic acid metabolism pathways were enriched in both SIX1 OE and 8430 treated conditions (Fig. 5b), suggesting SIX1 is involved in these metabolic processes.

Compound 8430 exhibits promising anti-metastatic potency *in vivo*, but the mechanism remains to be determined. *In vivo* target engagement and time of residency as well as the effect in other breast cancer models might be necessary to fully assess the therapeutic value of 8430. Remarkably, although treatment of 8430 was carried out only until day 21 in our *in vivo* metastasis experiment, enhanced junctional E-CAD was detected 6 weeks after 8430 treatment was discontinued, suggesting that 8430 imposed long-term (or irreversible) changes on tumor cells preventing them from readily going through EMT. SIX1 has been shown to mediate metastasis via both cell autonomous and non-cell autonomous means (11, 24, 27, 42), and its inhibition may thus change not only the tumor cells themselves, but also the tumor microenvironment, leading to more lasting effects. For example, high SIX1 expression in tumor cells induces lymphangiogenesis (23, 48) and angiogenesis (50), where the latter process can recruit tumor-associated macrophages to further foster tumor progression (50). Additionally, high SIX1 expression in macrophages promotes hepatocellular carcinoma growth and invasion (52). It is possible that 8430's anti-metastatic efficacy is partially attributed to creating an anti-metastatic microenvironment which has a prolonged effects on blocking tumor cell dissemination and colonization. Alternatively, loss of SIX1 may disable tumor cell plasticity, locking the cells in a more differentiated and less metastatic state.

Before 8430 can be moved into the clinical realm, significant chemical alterations are needed to improve the compound, including increased solubility and increased half-life *in vivo*. We anticipate that pharmacologically targeting the SIX1/EYA2 complex can potentially benefit patients whose cancers express high levels of SIX1 and EYA2 together. Because many studies have associated SIX1 with the induction of an EMT signature (11, 24, 42, 53) that is known to contribute to resistance to therapeutic regimens including tyrosine kinase inhibitors and immunotherapy (54), SIX1/EYA2 inhibitors may also serve as a promising adjuvant therapy to prolong patients' responses to other chemotherapeutic regimens.

Supplementary Material

Refer to Web version on PubMed Central for supplementary material.

Acknowledgements

We thank the Tissue Biobanking & Histology Shared Resource for immunohistochemistry and advice. We thank the Cancer Center Support Grant (P30CA046934) for supporting the following shared resources used in this work: Tissue Biobanking & Histology, Animal Imaging, Biostatistics and Bioinformatics, and Cell Technologies. We thank Marisa Elise Wagley and Emily Duncan for help making Figure 2c and Dr. Paul Jedlicka for confirming metastases in the described animal study. This work was supported in whole or in part by the following grants: NIH R01CA224867 (H.L. Ford and Michael T. Lewis), NIH R01NS108396 (H.L. Ford), NIH R03DA033174 (R. Zhao and H.L. Ford), NIH R21CA185752 (R. Zhao and H.L. Ford), AACR-BCRF grant 10–60-26-FORD (H.L. Ford), Alex's Lemonade Stand Foundation Innovation Grant (H.L. Ford), DOD Synergistic grant BC084105P1 (R. Zhao and H.L. Ford), the Colorado Cancer Translational Research Accelerator award (H.L. Ford and R. Zhao), Colorado Bioscience Discovery and Evaluation Grant (R. Zhao and H.L. Ford), Cancer League of Colorado Research Grant (R. Zhao and H.L. Ford), The V Foundation for Cancer Research Award (R. Zhao), Kimmel Foundation for Cancer Research grant (R. Zhao), and an NCI fellowship 1F99CA234940–01 to H. Zhou. Work at NCATS was supported by the NIH Intramural Research Program.

References

1. Gross S, Rahal R, Stransky N, Lengauer C & Hoeflich KP Targeting cancer with kinase inhibitors. J Clin Invest 125, 1780–1789 (2015). [PubMed: 25932675]
2. Zhang J, Yang PL & Gray NS Targeting cancer with small molecule kinase inhibitors. Nat Rev Cancer 9, 28–39 (2009). [PubMed: 19104514]
3. Pauken KE, Dougan M, Rose NR, Lichtman AH & Sharpe AH Adverse Events Following Cancer Immunotherapy: Obstacles and Opportunities. Trends Immunol 40, 511–523 (2019). [PubMed: 31053497]
4. Bradner JE, Hnisz D & Young RA Transcriptional Addiction in Cancer. Cell 168, 629–643 (2017). [PubMed: 28187285]
5. Blevins MA, Towers CG, Patrick AN, Zhao R & Ford HL The SIX1-EYA transcriptional complex as a therapeutic target in cancer. Expert Opin Ther Targets 19, 213–225 (2015). [PubMed: 25555392]
6. Micalizzi DS, Farabaugh SM & Ford HL Epithelial-mesenchymal transition in cancer: parallels between normal development and tumor progression. J Mammary Gland Biol Neoplasia 15, 117–134 (2010). [PubMed: 20490631]
7. Xu PX, et al. Six1 is required for the early organogenesis of mammalian kidney. Development 130, 3085–3094 (2003). [PubMed: 12783782]
8. Kingsbury TJ, Kim M & Civin CI Regulation of cancer stem cell properties by SIX1, a member of the PAX-SIX-EYA-DACH network. Adv Cancer Res 141, 1–42 (2019). [PubMed: 30691681]
9. Ono H, et al. SIX1 promotes epithelial-mesenchymal transition in colorectal cancer through ZEB1 activation. Oncogene 31, 4923–4934 (2012). [PubMed: 22286765]
10. Behbakht K, et al. Six1 overexpression in ovarian carcinoma causes resistance to TRAIL-mediated apoptosis and is associated with poor survival. Cancer Res 67, 3036–3042 (2007). [PubMed: 17409410]
11. Micalizzi DS, et al. The Six1 homeoprotein induces human mammary carcinoma cells to undergo epithelial-mesenchymal transition and metastasis in mice through increasing TGF-beta signaling. J Clin Invest 119, 2678–2690 (2009). [PubMed: 19726885]
12. Ng KT, et al. Clinicopathological significance of homeoprotein Six1 in hepatocellular carcinoma. British journal of cancer 95, 1050–1055 (2006). [PubMed: 17008870]
13. Ford HL, Kabingu EN, Bump EA, Mutter GL & Pardee AB Abrogation of the G2 cell cycle checkpoint associated with overexpression of HSIX1: a possible mechanism of breast carcinogenesis. Proc Natl Acad Sci U S A 95, 12608–12613 (1998). [PubMed: 9770533]
14. Walz AL, et al. Recurrent DGCR8, DROSHA, and SIX homeodomain mutations in favorable histology Wilms tumors. Cancer Cell 27, 286–297 (2015). [PubMed: 25670082]

15. Wegert J, et al. Mutations in the SIX½ pathway and the DROSHA/DGCR8 miRNA microprocessor complex underlie high-risk blastemal type Wilms tumors. Cancer Cell 27, 298–311 (2015). [PubMed: 25670083]
16. Li L, et al. Transcriptional Regulation of the Warburg Effect in Cancer by SIX1. Cancer Cell 33, 368–385 e367 (2018). [PubMed: 29455928]
17. Reichenberger KJ, Coletta RD, Schulte AP, Varella-Garcia M & Ford HL Gene amplification is a mechanism of Six1 overexpression in breast cancer. Cancer Res 65, 2668–2675 (2005). [PubMed: 15805264]
18. Iwanaga R, et al. Expression of Six1 in luminal breast cancers predicts poor prognosis and promotes increases in tumor initiating cells by activation of extracellular signal-regulated kinase and transforming growth factor-beta signaling pathways. Breast Cancer Res 14, R100 (2012). [PubMed: 22765220]
19. Coletta RD, et al. Six1 overexpression in mammary cells induces genomic instability and is sufficient for malignant transformation. Cancer Res 68, 2204–2213 (2008). [PubMed: 18381426]
20. McCoy EL, et al. Six1 expands the mouse mammary epithelial stem/progenitor cell pool and induces mammary tumors that undergo epithelial-mesenchymal transition. J Clin Invest 119, 2663–2677 (2009). [PubMed: 19726883]
21. Ng KT, et al. Suppression of tumorigenesis and metastasis of hepatocellular carcinoma by shRNA interference targeting on homeoprotein Six1. Int J Cancer (2009).
22. Yu Y, et al. Expression profiling identifies the cytoskeletal organizer ezrin and the developmental homeoprotein Six-1 as key metastatic regulators. Nat Med 10, 175–181 (2004). [PubMed: 14704789]
23. Wang CA, et al. SIX1 induces lymphangiogenesis and metastasis via upregulation of VEGF-C in mouse models of breast cancer. J Clin Invest 122, 1895–1906 (2012). [PubMed: 22466647]
24. Neelakantan D, et al. EMT cells increase breast cancer metastasis via paracrine GLI activation in neighbouring tumour cells. Nat Commun 8, 15773 (2017). [PubMed: 28604738]
25. Bushweller JH Targeting transcription factors in cancer - from undruggable to reality. Nat Rev Cancer 19, 611–624 (2019). [PubMed: 31511663]
26. Farabaugh SM, Micalizzi DS, Jedlicka P, Zhao R & Ford HL Eya2 is required to mediate the pro-metastatic functions of Six1 via the induction of TGF-beta signaling, epithelial-mesenchymal transition, and cancer stem cell properties. Oncogene 31, 552–562 (2012). [PubMed: 21706047]
27. Patrick AN, et al. Structure-function analyses of the human SIX1-EYA2 complex reveal insights into metastasis and BOR syndrome. Nat Struct Mol Biol 20, 447–453 (2013). [PubMed: 23435380]
28. Abdelhak S, et al. A human homologue of the Drosophila eyes absent gene underlies branchio-oto-renal (BOR) syndrome and identifies a novel gene family. Nature genetics 15, 157–164. (1997). [PubMed: 9020840]
29. Borsani G, et al. EYA4, a novel vertebrate gene related to Drosophila eyes absent. Human molecular genetics 8, 11–23 (1999). [PubMed: 9887327]
30. Zimmerman JE, et al. Cloning and characterization of two vertebrate homologs of the Drosophila eyes absent gene. Genome Res 7, 128–141 (1997). [PubMed: 9049631]
31. Zhang L, et al. Transcriptional coactivator Drosophila eyes absent homologue 2 is up-regulated in epithelial ovarian cancer and promotes tumor growth. Cancer Res 65, 925–932 (2005). [PubMed: 15705892]
32. Blevins MA, et al. Small Molecule, NSC95397, Inhibits the CtBP1-Protein Partner Interaction and CtBP1-Mediated Transcriptional Repression. J Biomol Screen 20, 663–672 (2015). [PubMed: 25477201]
33. Zhang L, et al. Eya3 partners with PP2A to induce c-Myc stabilization and tumor progression. Nat Commun 9, 1047 (2018). [PubMed: 29535359]
34. Love MI, Huber W & Anders S Moderated estimation of fold change and dispersion for RNA-seq data with DESeq2. Genome Biol 15, 550 (2014). [PubMed: 25516281]
35. Liberzon A, et al. Molecular signatures database (MSigDB) 3.0. Bioinformatics 27, 1739–1740 (2011). [PubMed: 21546393]

36. Yu G, Wang LG, Han Y & He QY clusterProfiler: an R package for comparing biological themes among gene clusters. OMICS 16, 284–287 (2012). [PubMed: 22455463]
37. Nemkov T, D'Alessandro A & Hansen KC Three-minute method for amino acid analysis by UHPLC and high-resolution quadrupole orbitrap mass spectrometry. Amino Acids 47, 2345–2357 (2015). [PubMed: 26058356]
38. Bielefeld-Sevigny M AlphaLISA immunoassay platform- the "no-wash" high-throughput alternative to ELISA. Assay Drug Dev Technol 7, 90–92 (2009). [PubMed: 19382891]
39. Spitz F, et al. Expression of myogenin during embryogenesis is controlled by Six/sine oculis homeoproteins through a conserved MEF3 binding site. Proc Natl Acad Sci U S A 95, 14220–14225 (1998). [PubMed: 9826681]
40. Greenwood C, et al. Proximity assays for sensitive quantification of proteins. Biomol Detect Quantif 4, 10–16 (2015). [PubMed: 27077033]
41. Hansen MC, Nederby L, Henriksen MO, Hansen M & Nyvold CG Sensitive ligand-based protein quantification using immuno-PCR: A critical review of single-probe and proximity ligation assays. Biotechniques 56, 217–228 (2014). [PubMed: 24919231]
42. Micalizzi DS, Wang CA, Farabaugh SM, Schiemann WP & Ford HL Homeoprotein Six1 increases TGF-beta type I receptor and converts TGF-beta signaling from suppressive to supportive for tumor growth. Cancer Res 70, 10371–10380 (2010). [PubMed: 21056993]
43. Nie ZY, et al. miR-140–5p induces cell apoptosis and decreases Warburg effect in chronic myeloid leukemia by targeting SIX1. Biosci Rep 39(2019).
44. Yang X, et al. MiR-150–5p regulates melanoma proliferation, invasion and metastasis via SIX1-mediated Warburg Effect. Biochem Biophys Res Commun 515, 85–91 (2019). [PubMed: 31128917]
45. Dongre A & Weinberg RA New insights into the mechanisms of epithelial-mesenchymal transition and implications for cancer. Nat Rev Mol Cell Biol 20, 69–84 (2019). [PubMed: 30459476]
46. Chen L, et al. cPLA2alpha mediates TGF-beta-induced epithelial-mesenchymal transition in breast cancer through PI3k/Akt signaling. Cell Death Dis 8, e2728 (2017). [PubMed: 28383549]
47. Mahdi SH, Cheng H, Li J & Feng R The effect of TGF-beta-induced epithelial-mesenchymal transition on the expression of intracellular calcium-handling proteins in T47D and MCF-7 human breast cancer cells. Arch Biochem Biophys 583, 18–26 (2015). [PubMed: 26247838]
48. Liu D, et al. SIX1 promotes tumor lymphangiogenesis by coordinating TGFbeta signals that increase expression of VEGF-C. Cancer Res 74, 5597–5607 (2014). [PubMed: 25142796]
49. Liu D, et al. Sine oculis homeobox homolog 1 promotes alpha5beta1-mediated invasive migration and metastasis of cervical cancer cells. Biochem Biophys Res Commun 446, 549–554 (2014). [PubMed: 24613848]
50. Xu H, Zhang Y, Pena MM, Pirisi L & Creek KE Six1 promotes colorectal cancer growth and metastasis by stimulating angiogenesis and recruiting tumor-associated macrophages. Carcinogenesis 38, 281–292 (2017). [PubMed: 28199476]
51. Pandey RN, et al. The Eyes Absent phosphatase-transactivator proteins promote proliferation, transformation, migration, and invasion of tumor cells. Oncogene 29, 3715–3722 (2010). [PubMed: 20418914]
52. Zhang Y, et al. Increased Six1 expression in macrophages promotes hepatocellular carcinoma growth and invasion by regulating MMP-9. J Cell Mol Med 23, 4523–4533 (2019). [PubMed: 31044528]
53. Xu H, et al. Six1 promotes epithelial-mesenchymal transition and malignant conversion in human papillomavirus type 16-immortalized human keratinocytes. Carcinogenesis 35, 1379–1388 (2014). [PubMed: 24574515]
54. Smith BN & Bhowmick NA Role of EMT in Metastasis and Therapy Resistance. J Clin Med 5(2016).

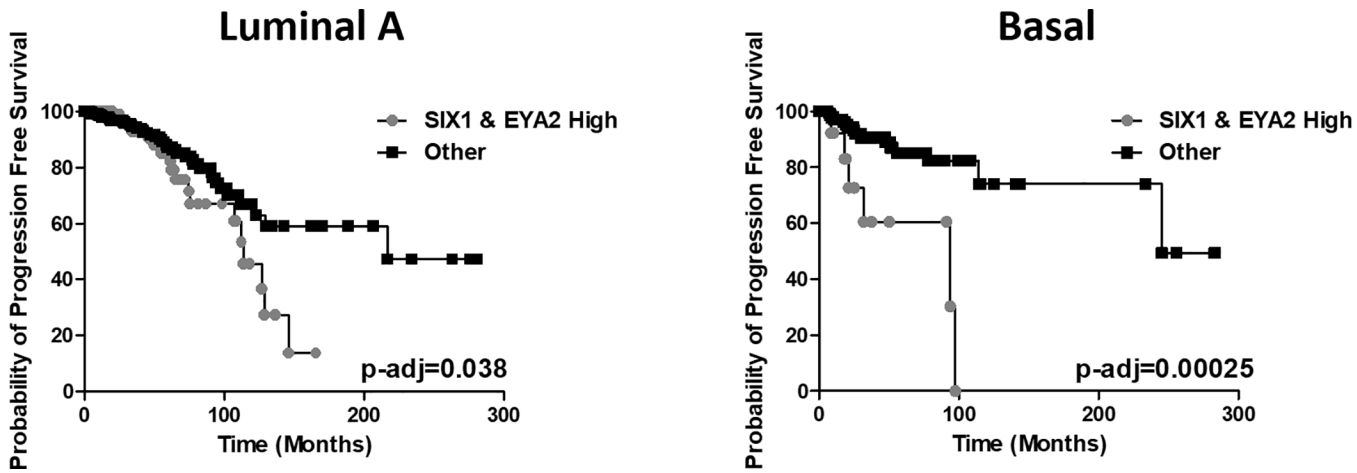

Figure 1. Concerted upregulation of SIX1 and EYA2 predicts poor survival in Luminal A and Basal subtype breast cancer patients.

Kaplan Meier curves of Luminal A (n=497) and Basal BRCA (n=171) patients based on $\log_2$ median SIX1 and EYA2 mRNA expression. The "SIX1 and EYA2 high" strata exhibited SIX1 and EYA2 mRNA expression higher than the 55^{th} percentile in the Luminal A group and the 74^{th} percentile in the Basal group. Adjusted p-values were calculated using a log-rank test with fitting under a Cox proportional hazards model.

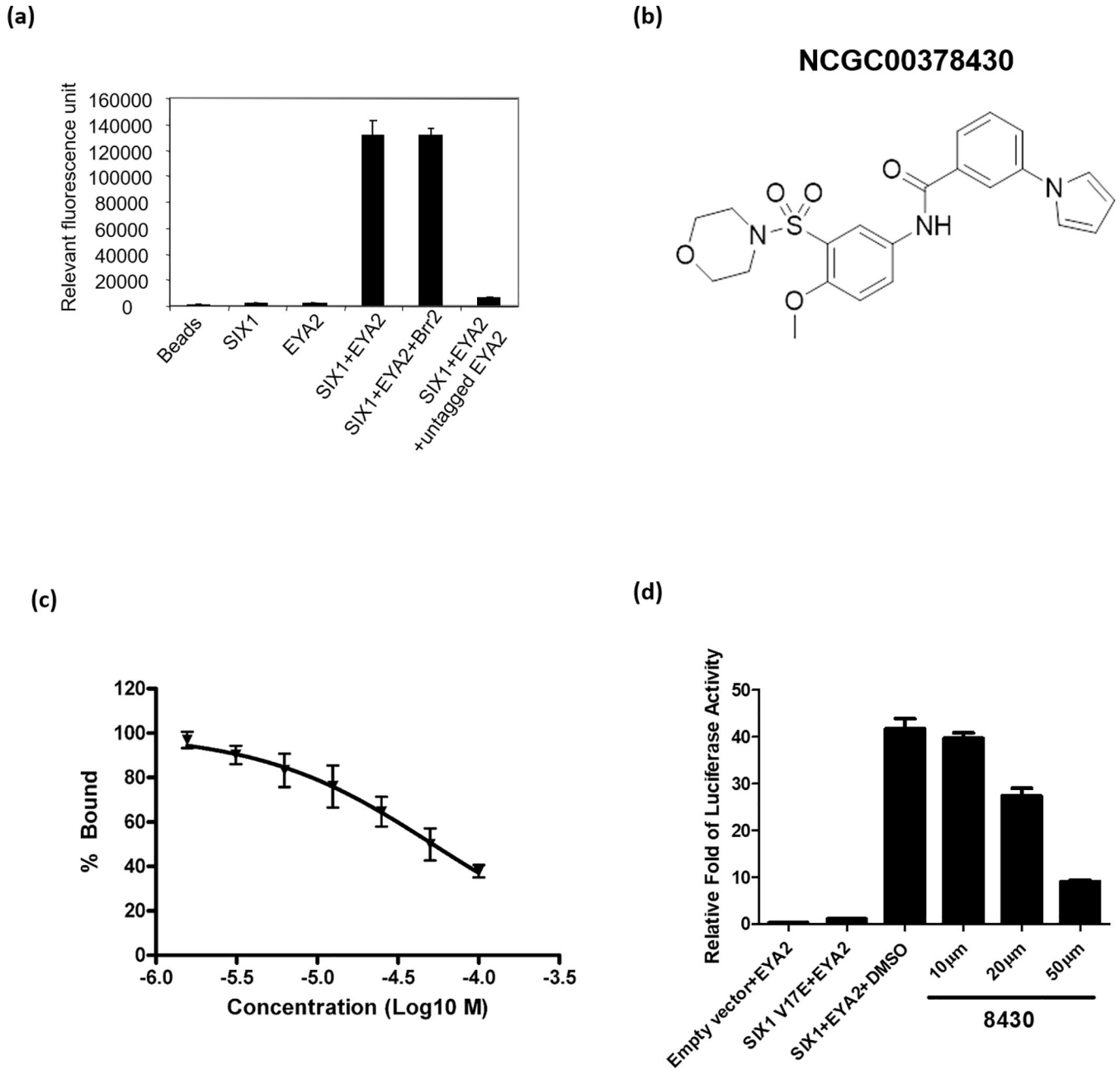

Figure 2. Compound 8430 disrupts SIX1-EYA2 interaction *in vitro*.

a. Incubation of GST-SIX1 with His-EYA2 results in significant AlphaScreen signal compared to AlphaScreen beads alone or incubated with each individual protein. Untagged EYA2, but not an unrelated protein, Brr2, competes for the tagged EYA2 protein and diminishes the AlphaScreen signal. **b.** Structures of compound NCGC00378430 (abbreviated as 8430). **c.** Dose response curve of compound 8430 in the AlphaScreen assay. **d.** Transcriptional activity of a MEF3 promoter luciferase reporter in the presence of EYA2 + an empty vector, EYA2 + SIX1 V17E mutant, EYA2 + SIX1 WT, and EYA2 + SIX1 WT + different concentrations of compound 8430.

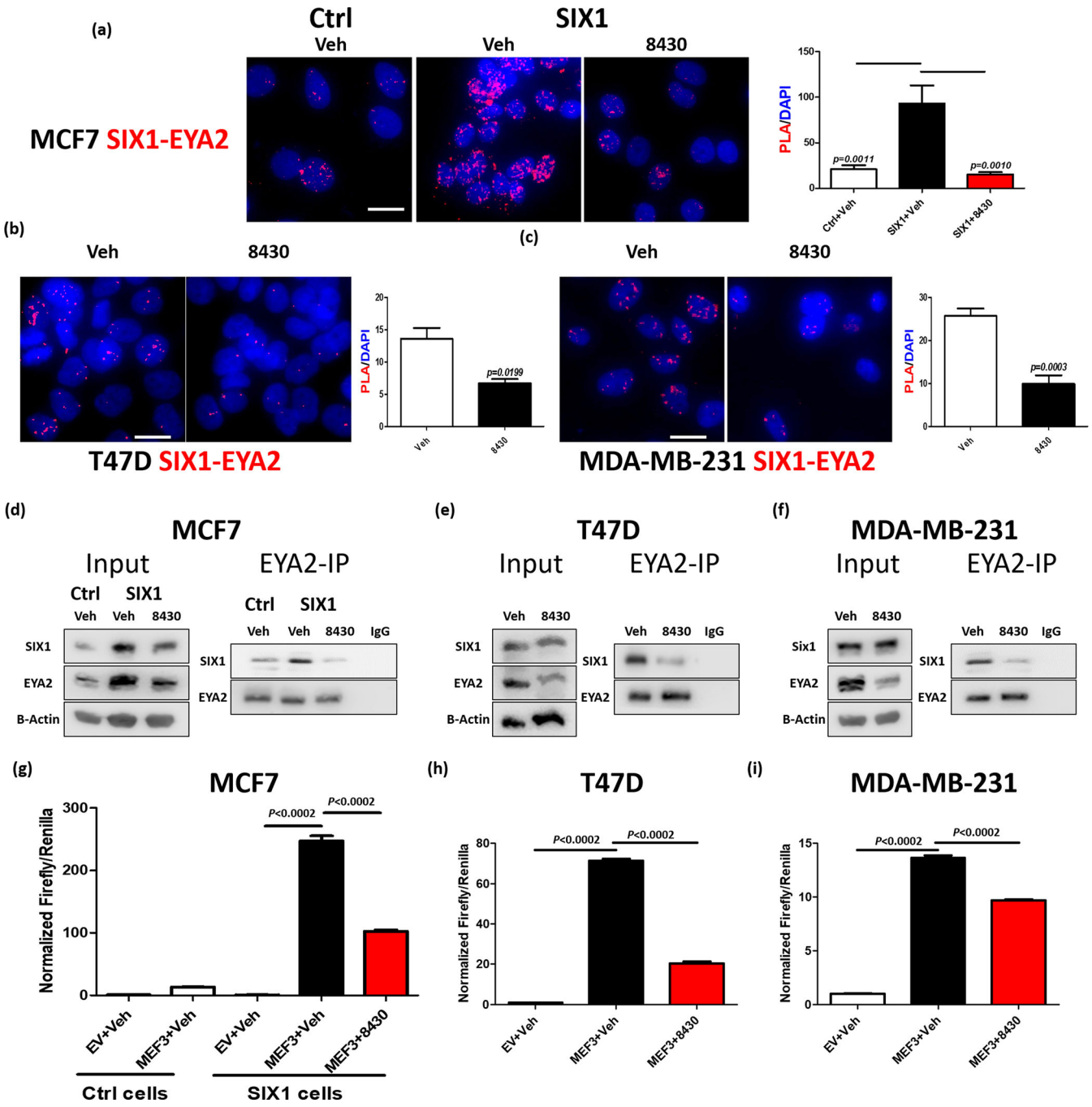

Figure 3. Compound 8430 disrupts SIX1-EYA2 interaction in breast cancer cells.

Representative images (n=4) of a Proximity Ligation Assay (PLA) assessing the SIX1-EYA2 interaction in MCF7-Ctrl and MCF7-SIX1 cells treated with vehichle (DMSO) or 10μM 8430 **(a)**, T47D cells treated with vehicle or 20μM 8430 **(b)**, and MDA-MB-231 cells treated with vehicle or 20μM 8430 **(c).** Scale bars=20μm. Graphs demonstrate the mean of PLA signal over the DAPI in representative experiments. Error bars represent standard deviation, and statistical significance was evaluated by one-way ANOVA followed by Tukey post adjustment (MCF7) or unpaired 2-tailed t-test (T47D and MDA MB 231), *p values are listed*

with 4 decimal places. **d-f.** EYA2 Immunoprecipitation (IP) followed by Western Blot (WB) analyses. Representative images (n=3) of WBs demonstrate levels of SIX1 and EYA2 in input and in the EYA2-IP fractions in vehicle vs 8430 treated MCF7-Ctrl/SIX1 **(d)**, T47D **(e)**, and MDA-MB-231 **(f)** cells. 8430 was used at 10μM in MCF7 cells and at 20μM in T47D and MDA-MB-231 cells. To measure effect of 8430 on transcriptional activity, MEF3 Firefly/Renilla dual luciferase reporter assay was performed using MCF7-Ctrl, MCF7-SIX1, T47D, and MDA-MB-231 cells, treated with either vehicle or 8430. Normalized Firefly/Renilla luciferase signal from representative experiments (n=3) was plotted in MCF7-Ctrl or MCF7-SIX1 **(g)**, T47D **(h)** and MDA-MB-231 **(i)** cells. Error bars are standard deviations, and statistical significance was evaluated by one-way ANOVA followed by Tukey post adjustment, *p values are listed with 4 decimal places.*

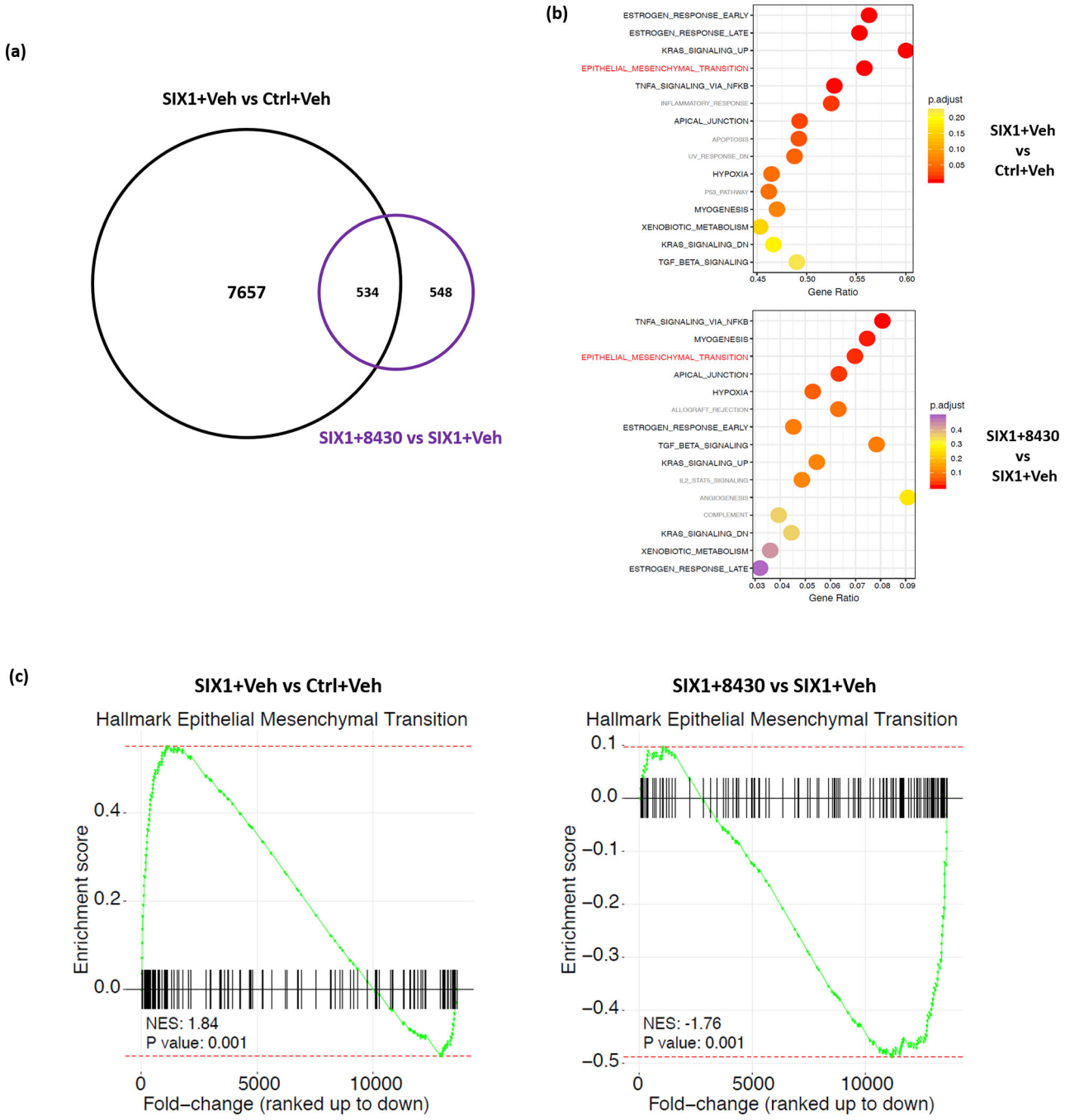

Figure 4. Compound 8430 partially reverses SIX1-mediated transcriptional signature.

RNA sequencing was conducted using total RNA isolated from 3 days of treatment as follows: MCF7-Ctrl+Vehicle (DMSO), MCF7-SIX1+Vehicle, and MCF7-SIX1+8430 (10μM). Each sample was analyzed in biological triplicates. **a.** Venn Diagram demonstrates the number of genes impacted by SIX1 overexpression (OE) and 8430 treatment, respectively. Genes that are upregulated with SIX1 OE and downregulated with 8430 treatment (or vice versa) are marked as overlap between the expression signatures. **b.** Over-representation analysis (ORA) was performed using genes identified to be differentially

expressed (p-adj <0.1). Dotplots demonstrate top 15 enriched hallmark pathways (ranked by adjusted *p* value), when comparing gene signatures of “SIX1+Vehicle” to “Ctrl+Vehicle” **(top)**, or “SIX1+8430” to “SIX1+Vehicle” **(bottom)**. Pathways that overlap or not overlap between the two graphs are labeled in black and grey, respectively, except for EMT, which is highlighted in red due to our focus on this pathway. **c.** Gene Set Enrichment Analysis (GSEA) was performed on ranked fold-change expression for SIX1+Veh to Ctrl+Veh **(left)** or SIX1+8430 to SIX1+Veh **(right)**, demonstrating that SIX1 OE and 8430 treatment influence genes involved in EMT.

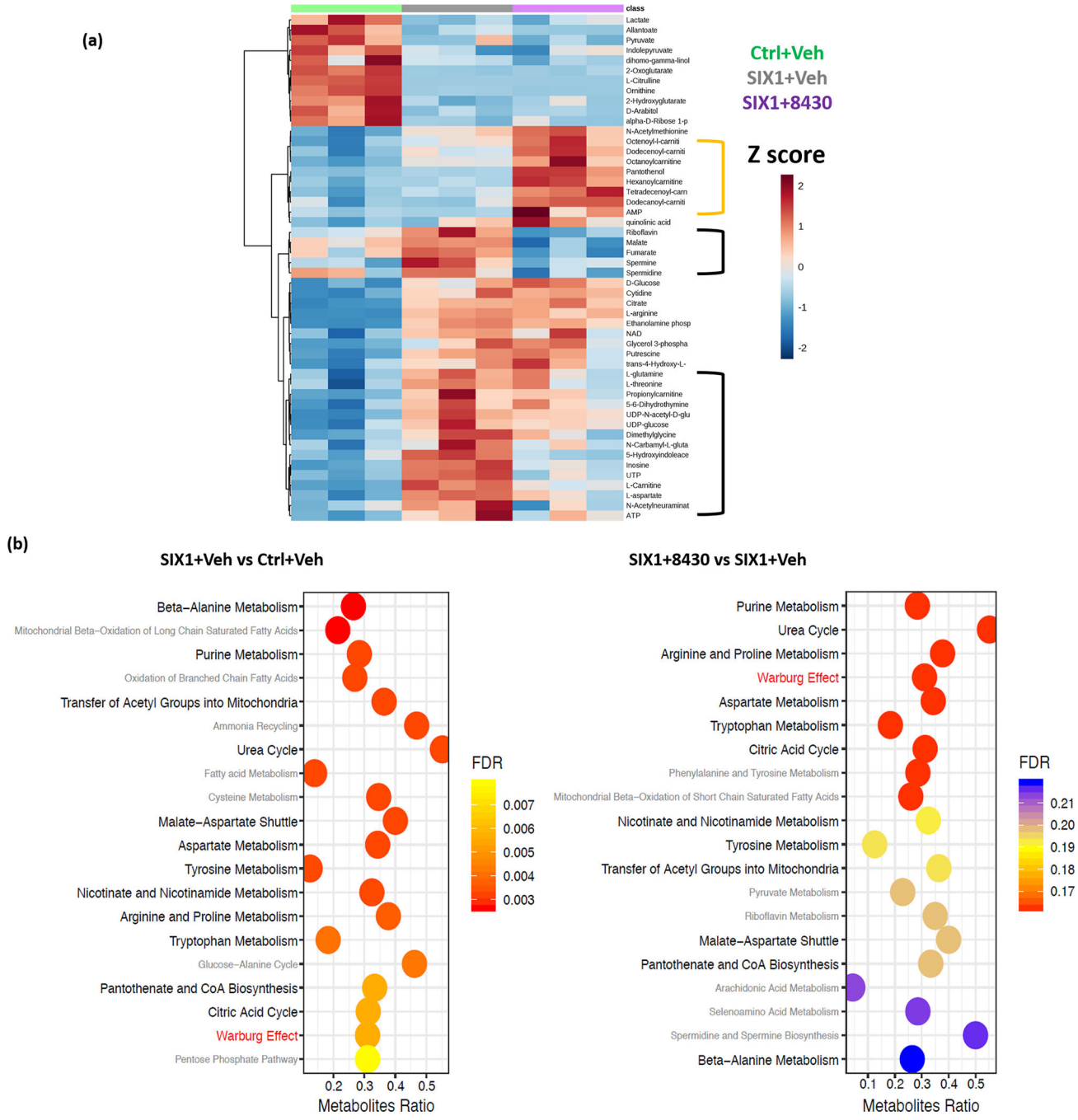

Figure 5. Compound 8430 partially reverses SIX1-mediated metabolic alterations.

Metabolomics analysis was conducted using cell lysates (biological triplicates) isolated after 3 days of treatment as follows: MCF7-Ctrl+Vehicle (DMSO), MCF7-SIX1+Vehicle, and MCF7-SIX1+8430 (10μM). **a.** Heatmap of top 50 most significantly changed metabolites by analysis of variance (ANOVA); metabolites that are altered by SIX1 and reversed by 8430 treatment are bracketed in black, while metabolites only altered by 8430 treatment is bracketed in yellow. **b.** Metabolite Set Enrichment Analysis (MSEA) was performed based on the relative quantitation of individual metabolites compared to the Small Molecule

Pathway DataBase (SMPDB). Bar graphs demonstrate top 20 enriched pathways (ranked by false discovery rate), when comparing gene signatures of “SIX1+Vehicle” to “Ctrl+Vehicle” **(left)**, or “SIX1+8430” to “SIX1+Vehicle” conditions **(right)**. Overlapping and non-overlapping pathways between the two graphs are labeled in black and grey, respectively, except the Warburg pathway which is labeled in red.

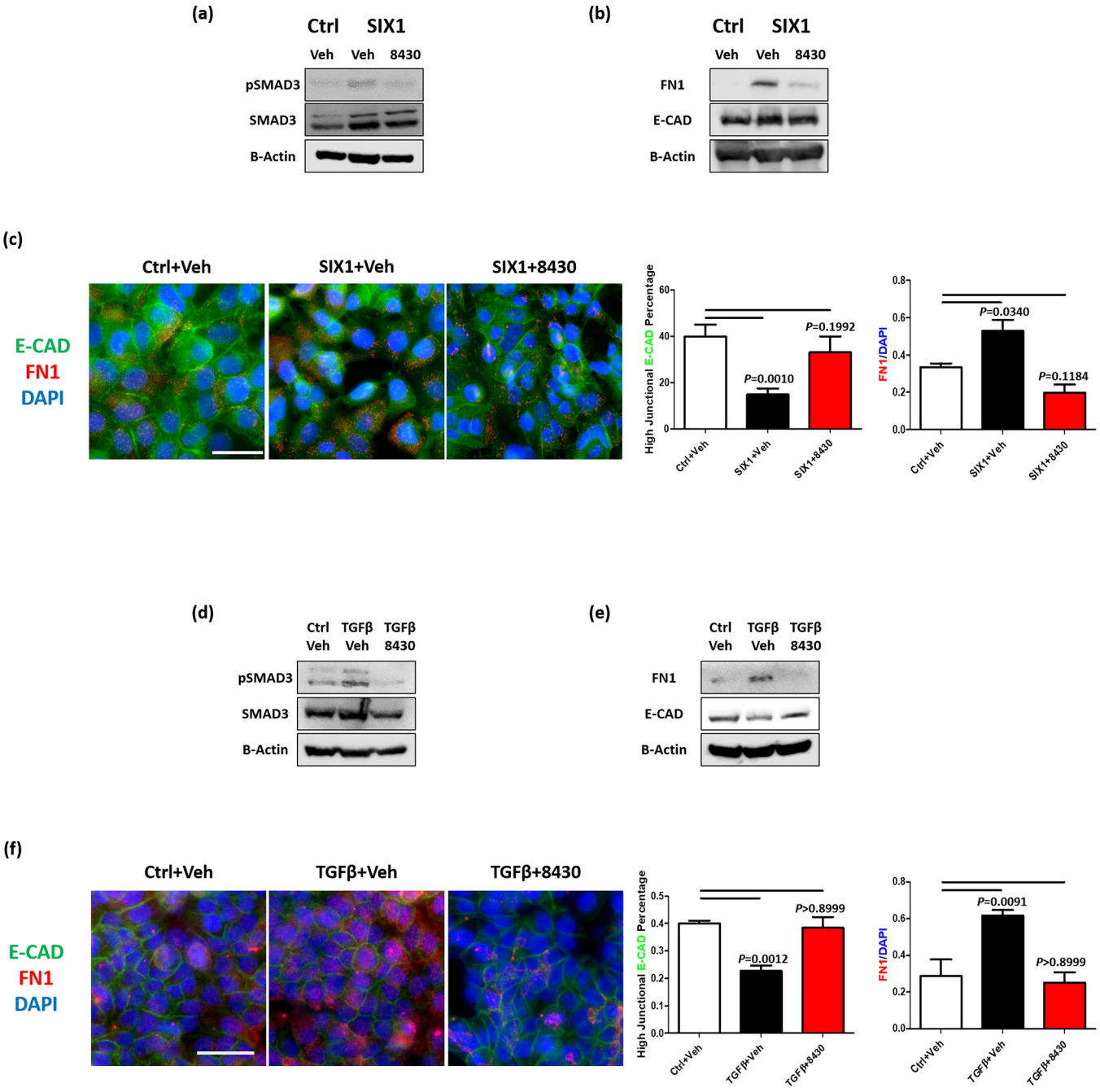

Figure 6. Compound 8430 inhibits TGF-β signaling and EMT in breast cancer cells with high SIX1 expression.

WB and immunocytochemistry (ICC) were performed using MCF7 or T47D cells after three days of treatment as follows: MCF7-Ctrl+vehicle (DMSO), MCF7-SIX1+vehicle, and MCF7-SIX1+8430 (10μM); T47D+Ctrl (PBS with 2mg/ml albumin)+vehicle, T47D+TGF-β1 (5ng/ml)+vehicle and T47D+TGF-β1 (5ng/ml)+8430 (20μM). Representative WB images (n=3) demonstrate protein levels of phospho-SMAD3, total SMAD3, fibronectin (FN1), and E-cadherin (E-CAD) in MCF7-Ctrl and MCF-SIX1 **(a, b)** and T47D **(d, e)** cells. Representative ICC images (n=4) demonstrate levels and distribution of E-CAD and FN1 in

MCF7-Ctrl and MCF7-SIX1 **(c)** and T47D **(f)** cells, scale bars=20μm. Percentage of cells with high junctional E-CAD and relative FN1 expression (normalized to DAPI stain) of the representative experiments are plotted on bar graphs. Error bars are standard deviations, and statistical significance was assessed by one-way ANOVA followed by Tukey post adjustment, *p values are listed with 4 decimal places.*

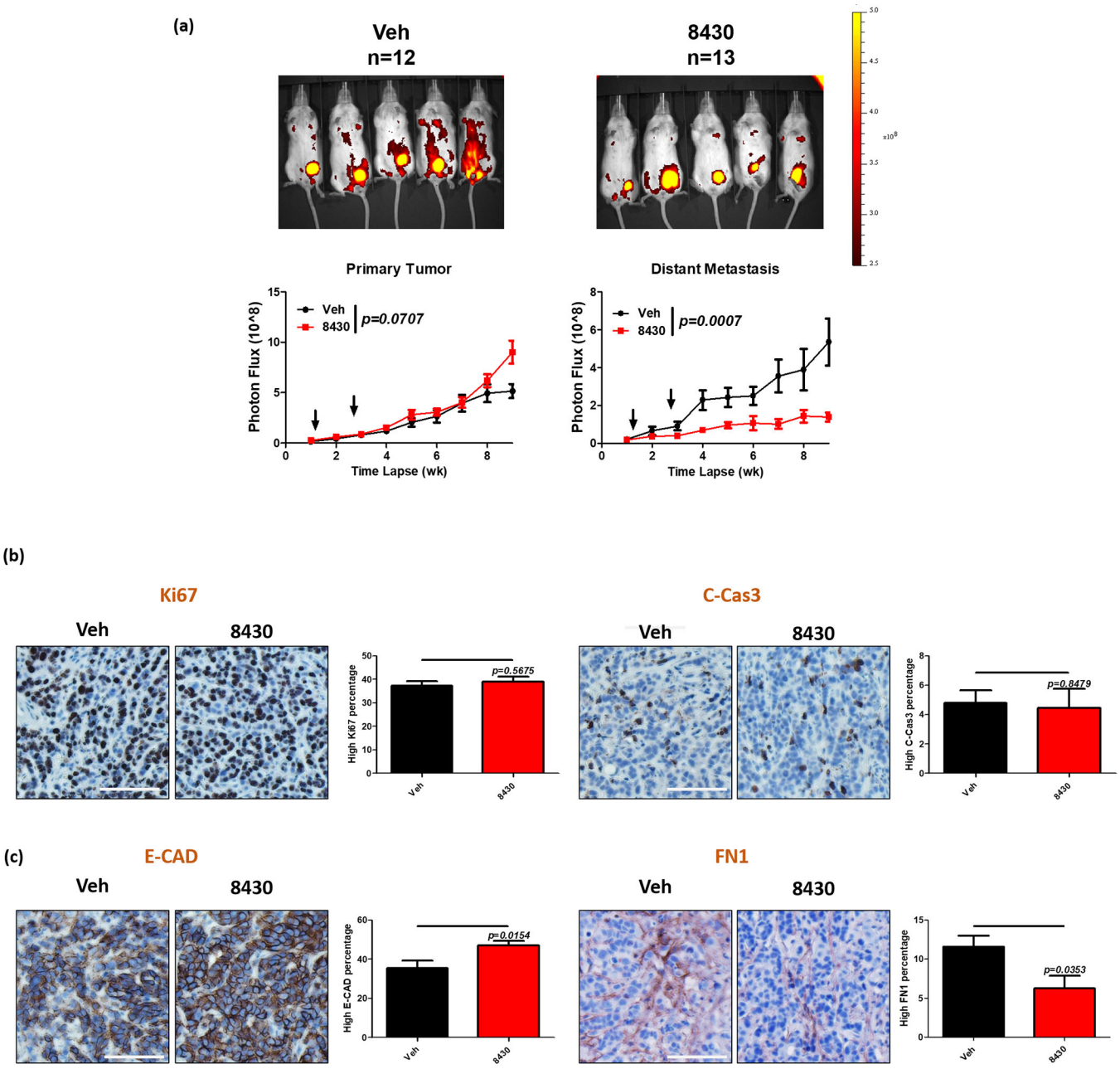

Figure 7. Compound 8430 inhibits metastasis of breast cancer cells expressing high levels of SIX1.

Mice carrying tRFP tagged MCF-SIX1 tumors were treated with either vehicle (NMP, PEG400 and 30% Solutol) or 25mg/kg of 8430 for 3 weeks (from day 3 to day 21). Primary tumors were harvested after week 9 for further immunohistochemical staining. **a.** Representative fluorescence images from week 9 are shown. Red fluorescence signal from primary tumors **(left)** and distant metastases **(right)** is quantitated and plotted over time in vehicle and 8430 treated mice. Arrows indicate the compound treatment duration. Error bars represent standard error of the mean, and statistical significance is assessed using a mixed-effects model. Representative IHC images for Ki67 **(b. left)**, Cleaved Caspase 3 **(b. right)**,

E-CAD **(c. left)** and FN1 **(c. right)**. Percentage of cells with high staining signal is plotted in bar graphs. Error bars represent standard error of the mean, and statistical significance was assessed using an unpaired 2-tailed t-test.